INTERNATIONAL JOURNAL OF CLIMATOLOGY
RMetS Royal Meteorological Society

The 'Warm-Arctic/Cold-Continents' pattern during 1901-2010

Journal:	*International Journal of Climatology*
Manuscript ID	JOC-17-0786.R1
Wiley - Manuscript type:	Research Article
Date Submitted by the Author:	20-Mar-2018
Complete List of Authors:	Chen, Linling; Nansen Environmental and Remote Sensing Center, Climate Dynamics and Prediction Francis, Jennifer; Rutgers The State University of New Jersey, Marine and Coastal Sciences Hanna, Edward; University of Lincoln, School of Geography and Lincoln Centre for Water and Planetary Health
Keywords:	Warm-Arctic, Cold-Continents, jet stream, blocking frequency/intensity, Arctic amplification, mid-latitude weather
Country Keywords:	Norway, United Kingdom Of Great Britain And Northern Ireland, United States

Title: The 'Warm-Arctic/Cold-Continents' pattern during 1901-2010

Running head: WACC pattern during 1920-1940 and 1990-2010

Linling CHEN[1], Jennifer FRANCIS[2], Edward HANNA[3]

[1]Nansen Environmental and Remote Sensing Centre and Bjerknes Centre for Climate Research, Norway

[2]Department of Marine and Coastal Sciences, Rutgers University, USA

[3]School of Geography and Lincoln Centre for Water and Planetary Health, College of Science, University of Lincoln, UK

The corresponding author: Linling Chen

Address: Thormøhlens gate 47, N-5006 Bergen, Norway

Email: linling.chen@nersc.no

Tel: +4755205800

Abstract. The 'Warm-Arctic/Cold-Continents' (WACC) winter weather pattern is investigated using the European Centre for Medium-Range Weather Forecasts 20th Century reanalysis data (ERA20C) spanning 1901-2010. Both the 1920-1940 and 1990-2010 periods are characterized by Arctic amplification (AA) and mid-latitude continental cooling, although the Arctic warming signal for 1990-2010 is twice as strong as that for 1920-1940. Significant weakening in the mid-latitude poleward temperature gradient and zonal wind, wavier upper-level flow character, and strong regional blocking frequency/intensity changes are also detected during both AA periods. These results based on statistical analyses highlight the possible role of AA in affecting mid-latitude weather patterns, but further work is needed to quantify the influence of AA on particular mid-latitude dynamical features.

Keywords

Warm-Arctic; Cold-Continents; jet stream; blocking frequency/intensity; Arctic amplification; mid-latitude weather

1. Introduction

The increase in near-surface air temperature observed in the Arctic since about 1990 has been almost twice as large as the global average: a phenomenon known as Arctic amplification, AA (Serreze et al., 2009; Screen and Simmonds, 2010; Wood and Overland, 2010; Cohen et al., 2014; Overland et al., 2016a). Both observational and modeling work have suggested that the AA, accompanied by melting Arctic sea ice and/or increasing Eurasian snow cover, may alter planetary-scale wave activity and the jet stream in the mid- and high latitudes (Honda et al., 2009; Cohen et al., 2013; Cohen

et al., 2014; Kim et al., 2014; Mori et al., 2014; Francis and Vavrus, 2015; Kretschmer et al., 2016; Pedersen et al., 2016; Wu and Smith, 2016; Zhang et al., 2016; Nakamura et al., 2016a; Nakamura et al., 2016b; Kretschmer et al., 2017; Vavrus et al., 2017). Thus AA may contribute to anomalous weather events in Northern Hemisphere (NH) mid-latitudes (Francis and Vavrus, 2012; Jaiser et al., 2012; Liu et al., 2012; Tang et al., 2013; Cohen et al., 2014; Wallace et al., 2014; Kug et al., 2015; Overland et al., 2015; Cohen, 2016; Overland et al., 2016b), and therefore offers a possible opportunity to improve extended-range seasonal forecasts for mid-latitudes (Garcia-Serrano and Frankignoul, 2014; Jung et al., 2014; Walsh, 2014).

Among these anomalous weather events, the 'Warm-Arctic/Cold-Continents' (WACC) temperature anomaly pattern (Overland et al., 2011) that has recently occurred frequently during NH winter (December-January-February, DJF) (Cohen et al., 2014; Shepherd, 2016; Cohen et al., 2018), is of particular interest, not only within the scientific community but also among the general public. WACC is a pattern that links the warm surface temperatures in the Arctic with cold continental winters. In extreme cases (e.g., periods in December 2016 and January 2017), the central Arctic was some 20°C warmer than normal in some areas while large parts of Siberia were around 20°C colder than the climatological mean for the period of 1979-2000 (http://cci-reanalyzer.org/reanalysis/daily_maps/, see the daily temperature anomaly maps). WACC has been associated with some exceptionally severe winter weather outbreaks along the US East Coast in the last decade (Cohen et al., 2018), and may even have affected peoples' perception of global warming (Capstick and Pidgeon, 2014; Hamilton and Lemcke-Stampone, 2014). Whether AA plays a key role in forcing the WACC pattern is still unclear (Overland et al., 2015; McCusker et al., 2016; Overland et al.,

2016b; Francis, 2017). One of the key challenges is that previous studies have generally focused on relatively short timespans (typically since around the mid-1990s), and have struggled to identify robust signals amid the substantial noise of natural variability (Cohen et al., 2014). More data (e.g., provided by recently-available centennial-timescale reanalysis datasets) are therefore needed before conclusions regarding climate impacts and feedbacks can be drawn with certainty (Hopsch et al., 2012).

Long-term observational records indicate that the WACC pattern occurred during the Early Twentieth Century Warming (1920s-1940s) as well as in the post-1990 period (Brönnimann et al., 2004; Johannessen et al., 2004; Cohen et al., 2010; Van Oldenborgh et al., 2015; Johannessen et al., 2016). This allows us to study the characteristics and factors influencing the WACC pattern during another historical period. Studies suggest that the earlier warming was mainly due to natural climate variability, while the recent surface air temperature changes are a response to anthropogenic forcing (Delworth and Knutson, 2000; Bengtsson et al., 2004; Johannessen et al., 2004; Yamanouchi, 2011; Thompson et al., 2015; Tokinaga et al., 2017). In this paper, we do not seek to directly address the causes of the WACC pattern, but instead we compare atmospheric dynamical features, including the poleward atmospheric temperature gradient, mid-latitude zonal wind, waviness of the jet stream, and blocking frequency/intensity, during these two AA periods. The similarities and differences help clarify whether the WACC pattern is mainly associated with either natural variability or anthropogenic forcing.

The paper is organized as follows: Data and methods are described in section 2. Changes in temperature, poleward temperature gradient, strength of zonal wind, upper-level flow character and blocking frequency/intensity in the periods of AA are presented in section 3. The main conclusions follow in section 4.

2. Data and methods

2.1 Data

The primary dataset used in this study is the European Centre for Medium-Range Weather Forecasts (ECMWF) 20th Century reanalysis, ERA20C (Poli et al., 2016). The source data are 6-hourly fields of 2-m air temperature, 1000- to 500-hPa (with 100-hPa interval) winds and geopotential height with a horizontal resolution of 1° latitude × 1° longitude for the period of 1900-2010 (https://www.ecmwf.int). Anomalies were calculated by subtracting the mean for each calendar day, averaged over 1981-2010, from each daily mean at each grid point, so that the climatological-mean seasonal cycle was removed. The key analyses are repeated using the following datasets:

1) the NASA Goddard Institute for Space Studies' observational surface temperature records, GISTEMP (Hansen et al., 2010) since 1880;

2) the ECMWF's coupled ocean-atmosphere reanalysis of the 20th century, CERA20C (Laloyaux et al., 2017), for the period 1900-2010;

3) the ECMWF's ERA-Interim reanalysis data (Dee et al., 2011) for the period since 1979;

4) NOAA 20th Century reanalysis version 2C, 20CRv2C (Compo et al., 2011), for the period since 1850.

Monthly surface temperature records from GISTEMP on a 2° latitude × 2° longitude grid with 250km smoothing were downloaded from http://www.esrl.noaa.gov/psd/; 6-hourly data of the same fields from CERA20C and ERA-interim were downloaded from https://www.ecmwf.int with the same horizontal resolution as the ERA20C; daily mean data from 20CRv2c with horizontal resolution of 2° × 2° were downloaded from http://www.esrl.noaa.gov/psd/. Anomalies relative to the common period of 1981-2010

were then calculated on a monthly basis for the GISTEMP, and on a daily basis for the other datasets.

2.2 MCI index

The Meridional Circulation Index (MCI) is used to measure atmospheric flow waviness (Francis and Vavrus, 2015). It is defined as the ratio of the meridional (north/south) wind component to the total wind speed:

$$MCI = \frac{v \times |v|}{u^2 + v^2}$$

where u and v are the zonal and meridional components of the wind. When $MCI = 0$, the wind is purely zonal, and when $MCI = 1(-1)$, the flow is from the south (north). The absolute value of MCI ($|MCI|$) gives the overall waviness of the flow, with a value close to 1(0) indicating predominantly meridional (zonal) flow (see Figure S6 in the supporting material: the DJF climatological mean of $|MCI|$ and 500hPa wind fields during 1901-2010). According to this definition, a more meridional flow can result from either a weaker u and/or stronger v wind component through simple vector geometry. Daily 500hPa wind components are used to calculate the MCI at each grid point in ERA20C reanalysis fields.

2.3 Blocking frequency/intensity

As an indicator of blocking, we have used a 2-D blocking index, which is an extension of the 1-D index defined by Tibaldi and Molteni (1990), referred to as the TM90 index. It is based on the reversal of the meridional gradient of 500hPa geopotential height (Z_{500}). Modifications as explained by Scherrer et al. (2006) are applied to the TM90 index. The geopotential height gradients (defined below) are calculated at central grid latitudes φ_c (varying between 35°N and 75° N, in 1° steps

135 with ERA20C data), with a distance of 15° between φ_c and the northern and southern
136 latitudes, φ_N and φ_S, respectively.

137 Specifically, for each grid point, we calculated the daily southern geopotential height
138 gradient (GHGS) and the northern geopotential height gradient (GHGN) as follows:

$$GHGS = \left(Z_{500}(\varphi_c) - Z_{500}(\varphi_c - 15°)\right)/15°$$

$$GHGN = \left(Z_{500}(\varphi_c + 15°) - Z_{500}(\varphi_c)\right)/15°$$

139 If the conditions GHGS > 0 and GHGN < -10 m per degree latitude are simultaneously
140 satisfied, a grid point is defined as instantaneously blocked. If the blocking occurs
141 within a box of 5°latitude × 10° longitude centered on that grid point for at least five
142 consecutive days, a blocking event is detected at that point (Davini et al., 2012). These
143 criteria ensure that the detected episodes have both significant meridional and zonal
144 extent, are quasi-stationary in space, and are continuous in time. This typically
145 corresponds to a mature blocking event.

146 The blocking frequency (BF) is then defined as the percentage of the number of
147 blocked days at a given grid point compared to the total number of winter days (90
148 days). This 2-D index has been widely used to investigate the NH blocking variability
149 (Rimbu and Lohmann, 2011; Davini et al., 2012; Rimbu et al., 2014; Kennedy et al.,
150 2016).

151 The blocking intensity (BI) index is used to quantify how much the atmospheric
152 circulation is affected by the presence of blocking. It is a 2-D extension of a BI index
153 defined by Lupo and Smith (1995). For each grid point where a blocking event is
154 detected:

$$BI(\lambda_0, \varphi_0) = 100 \times [(MZ \,/\, RC) - 1.0]$$

155 in which λ_0 and φ_0 represent the gridpoint's longitude and latitude, respectively. MZ is
156 the value of $Z_{500}(\lambda_0, \varphi_0)$. RC is the height of a subjectively chosen representative
157 contour with a slight modification made by Wiedenmann et al. (2002):

$$RC(\lambda_0, \varphi_0) = \frac{(Z_u + MZ)/2 + (Z_d + MZ)/2}{2}$$

158 where Z_u and Z_d represent the minimum of the Z_{500} field within 60° upstream and
159 downstream at the same latitude φ_0 of the chosen point, respectively. By definition, the
160 minimum value for BI is 0, and higher values indicate stronger events.

161 **2.4 Trend analysis**

162 We have extended the research period back to 1901 by using the century-long
163 reanalysis product from ERA20C. Linear trends in 2-m temperature, poleward
164 temperature gradient, zonal wind component, MCI, BF, and BI are calculated for the
165 periods of 1920-1940 (referred to as period AA1) and 1990-2010 (referred to as period
166 AA2). It should be noted that AA occurred not only during the AA1 and AA2 periods
167 but also in the 1950s-1960s, when the Arctic cooled faster than the NH lower latitudes
168 (Johannessen et al., 2016; Davy et al., 2017). However, since we are mainly concerned
169 with the WACC pattern, we naturally focus on the AA1 and AA2 Arctic warming
170 periods.

171 Trends are calculated using least square regression, and trends significantly different
172 from zero are identified using the Mann-Kendall (MK) test at the $\alpha = 0.05$ significance
173 level (Mann, 1945; Kendall, 1975). The possible effect of temporal autocorrelation on
174 trend detection (Yue et al., 2002) is considered, following the modification of the MK
175 test proposed by Yue and Wang (2004).
176

3. Results and discussion

3.1 Changes in temperature and poleward temperature gradient

WACC is a near-surface temperature anomaly pattern that depicts a relatively warm Arctic with cold continental winters. Cohen et al. (2014) used GISTEMP data and identified this pattern as positive temperature trends in the Arctic combined with negative trends in the NH mid-latitudes in general during 1990-2013. In our study, linear trends in 2-m temperature were calculated based on 90-day records in each DJF for the AA1 and AA2 periods.

The results indicate that the WACC pattern has appeared in the NH during both AA1 (Figure 1a) and AA2 (Figure 1b) periods. The mean DJF Arctic temperature (referred to as area-weighted average of temperature in the area of 0°-360°E, 60°-90°N) increased approximately 1.1°C per decade during the AA2 period, which is over twice as fast as during the AA1 period (0.5°C per decade). Although the ERA20C only assimilates surface pressure and marine wind observations, it represents the magnitude and variability of AA reasonably well (Figure S1a), and in general the difference between GISTEMP and reanalysis products is much smaller during the AA2 period (Figure S1b, c, d). This warming signal is particularly strong over Greenland, the Canadian Archipelago and Barents-Kara Seas. Conversely, the mid-latitude cooling signal is relatively strong in southern Europe and the Eurasian continent during the AA1 period, and in the United States and Eurasia during the AA2 period. This regional difference provides a good opportunity to study the WACC pattern in another historical period. As an additional comparison, we have applied a similar trend analysis (see details in section 2.4) to the GISTEMP, CERA20C, 20CRv2c and ERA-interim data. Figure S2 shows a similar WACC pattern during both AA periods in all datasets, but there are

larger differences between reanalyses and GISTEMP during the AA1 period. This is mostly likely due to the sparse observation during that period. The high density of observations during the AA2 period results in a better agreement between GISTEMP and reanalysis products (see Figure S2 b, d, f, h), whether they assimilate satellite observations (e.g., in ERA-interim) or only surface observations (e.g., in ERA20C, CERA20C and 20CRv2c).

AA also results in a smaller mid-latitude-to-pole temperature gradient, but the spatial distribution of the gradient varies regionally. In our study, the latitudinal thickness gradient (LTG) was extracted from vertically averaged 1000- to 500-hPa geopotential height daily fields from ERA20C. The LTG strength, i.e., the slope of the linear relationship between geopotential height and latitude (metres per latitude, referred to as m/lat) over every five grid points along the latitudinal line, is considered an alternative measure of poleward temperature gradient. Arguably thickness change is more relevant for assessing the effects of AA on the large-scale circulation (which will be our focus in section 3.2), as it represents warming over a deeper layer of the atmosphere that should more directly influence winds at upper levels (Francis and Vavrus, 2015). We then calculated the linear trend of the LTG for AA1 and AA2 periods (Figure 2). There is a significantly strong decrease in LTG between 45°N-65°N during both AA periods. The area is confined mainly to the central Atlantic sector during the AA1 period, but nearly the entire NH during the AA2 period. This may due to the fact that the AA signal is more pronounced in the Atlantic sector than in the Pacific sector during the AA1 period (Figure 1 and Figure S2, and also referring to Figure 2 in Wood and Overland (2010)).

3.2 Changes in zonal wind and upper-level flow character

Changes in poleward temperature or thickness gradients, according to the thermal wind relationship, affect the zonal wind speed. This means that in areas where the gradient increases (decreases), zonal winds strengthen (weaken), as shown by Francis and Vavrus (2015). Figure 3a,b demonstrate the significantly weakened zonal-mean zonal wind in all levels in the NH atmosphere, especially the upper troposphere, in both AA1 and AA2 periods. At the 500hPa level in both AA periods (Figure 3c,d), zonal wind weakening is greatest in the 45°N-65°N latitude belt, where the significant decrease of LTG is located (Figure 2). Again, the weakening of zonal wind is mainly seen in the Atlantic sector during the AA1 period.

Comparisons are also made with other reanalysis datasets. There is a good agreement among the reanalysis products on 500hPa zonal wind trends (Figure 3c,d, S3c,d, S4c,d, S5b); ERA20C shows stronger weakening of zonal mean zonal winds above 500hPa during the AA2 period, while CERA20C and 20CRv2c demonstrate closer pattern to ERA-interim (Figure 3b, S3b, S4b, S5a); Larger differences exist between 20CRv2c and (C)ERA20C for the AA1 period, namely stronger weakening of zonal mean zonal winds above 800hPa in the area north of 65°N in 20CRv2c (Figure 3a, S3a, S4a). This is probably because 20CRv2c does not assimilate any wind observations.

The changes in zonal wind strength will also affect the total wind direction. The MCI index was developed as an indication of the wind direction change (see the detailed description in section 2.2). Figure 4 presents the linear trends in DJF $|MCI|$ for winds at the 500hPa. The significant positive trends in $|MCI|$ indicate a shift in the wind vector to more meridional flow in NH mid-latitudes during both AA periods. This is also consistent with the locations where the LTG decreased (Figure 2) and where the u wind weakened (Figure 3 lower panel). However, a more meridional flow can result from

248 either a stronger *v* and/or weaker *u* wind component through simple vector geometry.
249 To discern whether a stronger *v* or weaker *u* plays the more important role, we fixed *u*
250 to its climatological mean (averaged for the period 1901-2010) in the MCI index
251 calculation (referred to as MCI*). This removes the widespread significant positive
252 trends shown in Figure 4b (Figure S7b), suggesting that the wavier flow at northern
253 mid-latitudes is mostly due to the weaker *u* wind component during the AA2 periods,
254 while the *v* wind component contributes over eastern Canada, southern Greenland and
255 Scandinavia during the AA1 period.

256 **3.3 Changes in blocking frequency and intensity**

257 Francis and Vavrus (2012) and Liu et al. (2012) suggested that reduced LTG would
258 change the mid-latitude atmospheric circulation by weakening the zonal winds and
259 increasing meridional flow, which would tend to result in a slower progression of
260 weather systems and more frequent atmospheric blocking events. These blockings, in
261 turn, play a key role in determining the mid-latitude weather, as shown in many
262 previous studies (Carrera et al., 2004; Luo et al., 2016; Chen and Luo, 2017; Xie and
263 Bueh, 2017). In this section, we will discuss the variability and trends in blocking
264 frequency and intensity in the NH during AA1 and AA2.

265 We introduced a 2-D blocking index (see description in section 2.3), and calculated
266 the corresponding BF as the percentage of the number of blocked days at a given grid
267 point per winter (90 days). Accordingly, we obtained 110 maps of BF of blocked grid
268 points, with one map per DJF for 1901-2010. Figure S8a displays the climatological
269 mean of these maps: 1) the well-known high-frequency areas present over North
270 Pacific-eastern Siberia, Greenland, Europe and Azores; and 2) two less pronounced
271 regions over the subtropical eastern Pacific and Ural Mountains. This is similar to the

BF maps based on other reanalysis datasets and/or other definitions of blocking in previous studies (Scherrer et al., 2006; Davini et al., 2012; Barnes et al., 2014; Rimbu et al., 2014).

There is no significant hemispheric-wide increase in BF during the AA1 and AA2, but clear regional trends include a general increase (decrease) in BF in the Atlantic (Pacific) sector north of 60°N (within the inner latitude circle in Figure 5a and 5b). Specifically, BF increased over the Atlantic sector (within a belt stretching from Greenland eastwards to Scandinavia), the Pacific sector (Alaska and western Siberia) and Ural Mountain area (Figure 5a and 5b). It also increased in central Europe in the AA1 period, and in subtropical eastern Pacific during the AA2 period. Given that only a few regions show trends above the 95% confidence level, the values shown in Figure 5b are consistent with Barnes et al. (2014), who found a significant increase in BF west of Greenland and over western Siberia, based on different reanalysis datasets and BF definitions during 1990-2012.

We also calculated the BI of these blocking events. Figure S8c shows that the climatological BI maxima appear at the exit area of both the Pacific and North Atlantic jet streams, and are not always collocated with the location of BF maxima: over eastern Siberia and Greenland, the BF values are high but BI values are low (in agreement with Davini et al. (2012)). Overall, the inter-annual variability (shown by the standard deviation of yearly values) of BI is relatively low compared with that of BF (Figure S8b,d). BI measures how much the circulation is affected by the existence of blocking, thus changes in BI may well be associated with the changes of strength and shape of the upper-level flow.

There are regional trends in BI, as well. Specifically, the combination of the BI and BF trend patterns indicate that: 1) during both AA periods (Figure 5), stronger blocking events tend to happen more frequently in the area between Greenland and central Europe, over the Ural Mountains, and in western Siberia; weaker events tend to happen less often over eastern Siberia; and 2) during the AA2 period (Figure 5b,d), weaker events tend to occur less often in central Europe. These results are in accordance with stronger blocking since 1990 in the context of a 165-year Greenland Blocking Index record (Hanna et al., 2016; Hanna et al., 2018), although the increase they reported is focused in summer (but is still evident in AA2 for winter). Davini et al. (2012) suggested that the increase/decrease dipole trends pattern in BF/BI in the Pacific sector is probably associated with an eastward shift of the Aleutian Low center (Overland et al., 1999). These clear regional features of BF/BI trends indicate that attempts to analyze the large area-averaged BF variations, e.g., Barnes et al. (2014), may obscure regional changes. The results mentioned above depend on the accuracy of Z_{500} in the reanalysis data. Since ERA20C only assimilates surface observations, we have also made a comparison of the BF/BI trends during the AA2 period with ERA-interim. Figure S9 shows very similar trends as those presented in Figure 5b,d, but with a more pronounced increase of BI over Greenland in AA2.

The increased frequency of stronger blocking events over the Atlantic sector, Ural Mountains, and western Siberia may have resulted in more mid-latitude WACC patterns in DJF during the AA2 period (Overland et al., 2015; Luo et al., 2016; Chen and Luo, 2017). On the other hand, the changes in low-latitude (e.g., south of 45°N) blockings may have a negligible impact on weather patterns because they are unable to block or divert the main polar jet-stream flow (according to Davini et al. (2012)).

It should be mentioned that some model-based studies (Hassanzadeh et al., 2014; Woollings et al., 2014; Kennedy et al., 2016) suggested a weak or even negligible Arctic influence on mid-latitude blockings. This can partly be explained by the fact that blocking features are still poorly simulated by many models (Anstey et al., 2013; Zappa et al., 2014; Davini and D'Andrea, 2016), and the preferred locations for blocks may be shifting (Masato et al., 2013). In addition, there is more than one metric to assess changes in NH blocking (Barnes et al., 2014), and one should be careful when making direct comparisons among results from dissimilar approaches. For example, Hassanzadeh et al. (2014) used idealized models to investigate the variations of blocked-area-per-day at each latitude, and concluded that the weakened poleward temperature gradient results in a robust decrease in blockings; however, decreased blocked-area does not necessarily mean decreased blocking frequency. Furthermore, (Yao et al., 2017) found that while blocks had generally weakened in Eurasia, they had also become more persistent, which will result in longer-lived weather regimes.

4. Summary and conclusions

In this paper, the DJF WACC pattern for 1901-2010 has been investigated based on a set of statistical diagnostics using ERA20C reanalysis products. Rapid Arctic warming accompanied by severe winters in the mid-latitudes is clearly shown in both AA1 and AA2 periods. Warming is especially strong in Greenland, the Canadian Archipelago, and the Barents-Kara sea area in both AA periods, while strong cooling is shown for southern Europe and the Eurasian continent during the AA1 period, and in the United States and Eurasia during the AA2 period. We cannot yet say whether the Arctic serves as an amplifier or a driver of these cold extremes owing to the challenge of detecting

343 robust atmospheric responses to AA within a short AA period. However, this study
344 provides comparative analyses of the WACC pattern in two historical periods of AA.
345 In terms of large-scale dynamical features, our statistical analysis demonstrates a
346 significant decrease in poleward temperature gradient and zonal wind strength between
347 45°N-65°N during both AA periods, which is prominent mainly in the Atlantic sector
348 during the AA1 period. Accordingly, trends in the absolute value of MCI indicate a
349 more meridional jet stream in the same latitudinal belt. While there is no significant
350 hemispheric-wide increase in BF or BI, the regional features in the blocking trends
351 reveal that stronger blocking events tend to happen more frequently in some high
352 latitudes regions (i.e., over North Atlantic sector, Ural Mountains, and western Siberia).
353 The main results have been replicated using GISTEMP, CERA20c, 20CRv2c and
354 ERA-interim data. Although the ERA20C only assimilates surface pressure and marine
355 wind observations, it represents the magnitude of WACC pattern, 500hpa *u* wind trends
356 and the BF/BI trends reasonably well. Especially during the AA2 period, there is a good
357 agreement among results from different datasets, whether they assimilate satellite
358 observations (e.g., in ERA-interim) or only surface observations (e.g., in ERA20C,
359 CERA20C and 20CRv2c).
360 We have not directly addressed the causes of the WACC pattern during these
361 periods. Some studies suggested a connection to the Arctic sea-ice decline (Honda et al.,
362 2009; Liu et al., 2012; Outten and Esau, 2012; Mori et al., 2014; Kug et al., 2015;
363 Semenov, 2016; Cohen et al., 2018), but other studies find no significant contributions
364 from sea ice (Woollings et al., 2014; Li et al., 2015; McCusker et al., 2016; Sun et al.,
365 2016). In some cases, the WACC pattern is a result of forcing both from the Arctic and
366 the lower latitudes (Lee et al., 2015; Francis et al., 2017). On multi-decadal timescales,

Atlantic Multidecadal Variability also plays important role (Semenov and Bengtsson, 2003; Keenlyside and Omrani, 2014; Peings and Magnusdottir, 2014). Probably there is no simple cause-and-effect path way in interpreting atmospheric dynamics, because the response of atmospheric circulation to the AA and other factors is essentially nonlinear (Petoukhov and Semenov, 2010; Semenov and Latif, 2015; Overland et al., 2016b).

It is worth highlighting that the linear trends in many of these dynamical features are comparable in terms of magnitude, but noticeably different in spatial distribution between the AA1 and AA2 period. This may partly due to the fact that the causal forcings of AA are different for these two periods, as mentioned in the introduction. It also suggests the need for a more in-depth dynamical meteorological investigation of regional mechanisms of AA and mid-latitude weather linkages.

Acknowledgements. The Research Council of Norway supported this study through the 'EuropeWeather' project (no. 231322 / F20, 'Does the Arctic sea--ice loss have an impact on the winter weather patterns in Europe?'). NordForsk also supported this study through the project GREENICE (61841): Impacts of Sea-Ice and Snow-Cover Changes on Climate, Green Growth, and Society. The authors thank two anonymous reviewers for constructive suggestions that improved the manuscript.

Supporting Information

The following supporting information is available as part of the article:

Figure S1. The area-weighted mean of 2-m air temperature anomalies in the area of 0°-360°E, 60°-90°N relative to the mean over the period of 1981-2010. This is shown as

a comparison between GISTEMP (black line) and reanalysis products (red line) from (a) ERA20C, (b) CERA20C, (c) 20CRv2c and (d) ERA-interim.

Figure S2. Trends in DJF temperature over the AA1 (left column) and AA2 (right column) periods from (a, b) GISTEMP, (c, d) CERA20C, (e, f) 20CRv2c and (g, h) ERA-interim. Units: °C per decade. The two black circles denote the 30°N and 60°N latitudes. Only trends above the 95% confidence level are plotted in (c), (d), (e), (f), (h). In (a) and (b), black dots indicate the area where trends are above the 95% confidence level, and blank areas denote missing value.

Figure S3. Same as Figure 3, but for CERA20C.

Figure S4. Same as Figure 3, but for 20CRv2c.

Figure S5. Same as Figure 3, but for ERA-interim during the AA2 period.

Figure S6. NH DJF climatological mean of |MCI| and 500hPa wind fields during 1901-2010.

Figure S7. Trends in DJF $|MCI^*|$ (u held constant) over the AA1 (a) and AA2 (b) periods, with only trends above the 95% confidence level plotted. Units: $|MCI^*|$value per decade. The two black circles denote the 30°N and 60°N latitudes.

Figure S8. DJF BF (a) and BI (c) climatology for the period of 1901-2010. Units are percentage of blocked days in the total number of days per season and BI value per season, respectively. (b) and (d) are the standard deviation of BF and BI. Note that 1% BF corresponds to about one blocked day per season. Only values where BF exceeds 1% are plotted. The two black circles denote the 30°N and 60°N latitudes.

Figure S9. Same as Figure 5, but for ERA-interim during the AA2 period.

References

Anstey JA, Davini P, Gray LJ, Woollings TJ, Butchart N, Cagnazzo C, Christiansen B, Hardiman SC, Osprey SM, Yang S. 2013. Multi□model analysis of Northern Hemisphere winter blocking: Model biases and the role of resolution. Journal of Geophysical Research: Atmospheres 118(10): 3956-3971.

Barnes EA, Dunn□Sigouin E, Masato G, Woollings T. 2014. Exploring recent trends in Northern Hemisphere blocking. Geophysical Research Letters 41(2): 638-644.

Bengtsson L, Semenov VA, Johannessen OM. 2004. The early twentieth-century warming in the Arctic-A possible mechanism. Journal of Climate 17(20): 4045-4057.

Brönnimann S, Luterbacher J, Staehelin J, Svendby T, Hansen G, Svenøe T. 2004. Extreme climate of the global troposphere and stratosphere in 1940–42 related to El Nino. Nature 431(7011): 971-974.

Capstick SB, Pidgeon NF. 2014. Public perception of cold weather events as evidence for and against climate change. Climatic Change 122(4): 695-708.

Carrera M, Higgins R, Kousky V. 2004. Downstream weather impacts associated with atmospheric blocking over the northeast Pacific. Journal of Climate 17(24): 4823-4839.

Chen X, Luo D. 2017. Arctic sea ice decline and continental cold anomalies: Upstream and downstream effects of Greenland blocking. Geophysical Research Letters 44(7): 3411-3419.

Cohen J, Foster J, Barlow M, Saito K, Jones J. 2010. Winter 2009–2010: A case study of an extreme Arctic Oscillation event. Geophysical Research Letters 37(17).

435 Cohen J, Jones J, Furtado JC, Tziperman E. 2013. Warm Arctic, cold continents a
436 common pattern related to Arctic sea ice melt, snow advance, and extreme winter
437 weather. Oceanography 26(4): 152-160.
438 Cohen J, Screen JA, Furtado JC, Barlow M, Whittleston D, Coumou D, Francis J,
439 Dethloff K, Entekhabi D, Overland J. 2014. Recent Arctic amplification and
440 extreme mid-latitude weather. Nature geoscience 7(9): 627-637.
441 Cohen J. 2016. An observational analysis: Tropical relative to Arctic influence on
442 midlatitude weather in the era of Arctic amplification. Geophysical Research
443 Letters 43: 5287–5294, doi: 10.1002/2016GL069102.
444 Cohen J, Pfeiffer K, Francis JA. 2018. Warm Arctic episodes linked with increased
445 frequency of extreme winter weather in the United States. Nature Communications
446 9(1): 869.
447 Compo GP, Whitaker JS, Sardeshmukh PD, Matsui N, Allan RJ, Yin X, Gleason BE,
448 Vose RS, Rutledge G, Bessemoulin P. 2011. The twentieth century reanalysis
449 project. Quarterly Journal of the Royal Meteorological Society 137(654): 1-28, doi:
450 10.1002/qj.776.
451 Davini P, Cagnazzo C, Gualdi S, Navarra A. 2012. Bidimensional diagnostics,
452 variability, and trends of Northern Hemisphere blocking. Journal of Climate
453 25(19): 6496-6509.
454 Davini P, D'Andrea F. 2016. Northern Hemisphere Atmospheric Blocking
455 Representation in Global Climate Models: Twenty Years of Improvements? Journal
456 of Climate 29(24): 8823-8840.
457 Davy R, Chen L, Hanna E. 2017. Arctic amplification metrics. International Journal of
458 Climatology. (under review).

459 Dee DP, Uppala S, Simmons A, Berrisford P, Poli P, Kobayashi S, Andrae U,
460 Balmaseda M, Balsamo G, Bauer P. 2011. The ERA□Interim reanalysis:
461 Configuration and performance of the data assimilation system. Quarterly Journal
462 of the royal meteorological society 137(656): 553-597.
463 Delworth TL, Knutson TR. 2000. Simulation of early 20th century global warming.
464 Science 287(5461): 2246-2250.
465 Francis JA, Vavrus SJ. 2012. Evidence linking Arctic amplification to extreme weather
466 in mid□latitudes. Geophysical Research Letters 39(6).
467 Francis JA, Vavrus SJ. 2015. Evidence for a wavier jet stream in response to rapid
468 Arctic warming. Environmental Research Letters 10(1): 014005.
469 Francis JA. 2017. Why Are Arctic Linkages to Extreme Weather Still Up in the Air?
470 Bulletin of the American Meteorological Society, doi: 10.1175/bams-d-17-0006.1.
471 Francis JA, Vavrus SJ, Cohen J. 2017. Amplified Arctic warming and mid□latitude
472 weather: new perspectives on emerging connections. Wiley Interdisciplinary
473 Reviews: Climate Change 8(5).
474 Garcia-Serrano J, Frankignoul C. 2014. High predictability of the winter Euro-Atlantic
475 climate from cryospheric variability. Nature Geoscience 7(6): E1-E1.
476 Hamilton LC, Lemcke□Stampone M. 2014. Arctic warming and your weather: public
477 belief in the connection. International Journal of Climatology 34(5): 1723-1728.
478 Hanna E, Cropper TE, Hall RJ, Cappelen J. 2016. Greenland Blocking Index 1851–
479 2015: a regional climate change signal. International Journal of Climatology
480 36(15): 4847-4861.
481 Hanna E, Hall RJ, Cropper TE, Ballinger TJ, Wake L, Mote T, Cappelen J. 2018.
482 Greenland Blocking Index daily series 1851-2015: analysis of changes in extremes

and links with North Atlantic and UK climate variability and change. International Journal of Climatology: In press.

Hansen J, Ruedy R, Sato M, Lo K. 2010. Global surface temperature change. Reviews of Geophysics 48(4).

Hassanzadeh P, Kuang Z, Farrell BF. 2014. Responses of midlatitude blocks and wave amplitude to changes in the meridional temperature gradient in an idealized dry GCM. Geophysical Research Letters 41(14): 5223-5232.

Honda M, Inoue J, Yamane S. 2009. Influence of low Arctic sea□ice minima on anomalously cold Eurasian winters. Geophysical Research Letters 36(8).

Hopsch S, Cohen J, Dethloff K. 2012. Analysis of a link between fall Arctic sea ice concentration and atmospheric patterns in the following winter. Tellus A: Dynamic Meteorology and Oceanography 64(1), doi: 10.3402/tellusa.v64i0.18624.

Jaiser R, Dethloff K, Handorf D, Rinke A, Cohen J. 2012. Impact of sea ice cover changes on the Northern Hemisphere atmospheric winter circulation. Tellus A: Dynamic Meteorology and Oceanography 64, doi: 10.3402/tellusa.v64i0.11595.

Johannessen OM, Bengtsson L, Miles MW, Kuzmina SI, Semenov VA, Alekseev GV, Nagurnyi AP, Zakharov VF, Bobylev LP, Pettersson LH. 2004. Arctic climate change: Observed and modelled temperature and sea□ice variability. Tellus A: Dynamic Meteorology and Oceanography 56(4): 328-341.

Johannessen OM, Kuzmina SI, Bobylev LP, Miles MW. 2016. Surface air temperature variability and trends in the Arctic: new amplification assessment and regionalisation. Tellus A: Dynamic Meteorology and Oceanography 68, doi: 10.3402/tellusa.v68.28234.

506 Jung T, Kasper MA, Semmler T, Serrar S. 2014. Arctic influence on subseasonal
507 midlatitude prediction. Geophysical Research Letters 41(10): 3676-3680.
508 Keenlyside N, Omrani N-E. 2014. Has a warm North Atlantic contributed to recent
509 European cold winters? Environmental Research Letters 9(6): 061001.
510 Kendall MG, 1975: Rank Correlation Methods, 4th ed., Charles Griffin. London.
511 Kennedy D, Parker T, Woollings T, Harvey B, Shaffrey L. 2016. The response of
512 high□impact blocking weather systems to climate change. Geophysical Research
513 Letters 43(13): 7250-7258.
514 Kim B-M, Son S-W, Min S-K, Jeong J-H, Kim S-J, Zhang X, Shim T, Yoon J-H. 2014.
515 Weakening of the stratospheric polar vortex by Arctic sea-ice loss. Nature
516 communications 5, doi: 10.1038/ncomms5646.
517 Kretschmer M, Coumou D, Donges JF, Runge J. 2016. Using causal effect networks to
518 analyze different Arctic drivers of midlatitude winter circulation. Journal of
519 Climate 29(11): 4069-4081.
520 Kretschmer M, Coumou D, Agel L, Barlow M, Tziperman E, Cohen J. 2017. More-
521 Persistent Weak Stratospheric Polar Vortex States Linked to Cold Extremes.
522 Bulletin of the American Meteorological Society, doi: 10.1175/bams-d-16-0259.1.
523 Kug J-S, Jeong J-H, Jang Y-S, Kim B-M, Folland CK, Min S-K, Son S-W. 2015. Two
524 distinct influences of Arctic warming on cold winters over North America and East
525 Asia. Nature Geoscience 8(10): 759, doi: 10.1038/ngeo2517.
526 Laloyaux P, De Boisseson E, Dahlgren P. 2017. CERA-20C: An Earth system approach
527 to climate reanalysis. EC MWF Newsletter(150): 25-30.
528 Lee MY, Hong CC, Hsu HH. 2015. Compounding effects of warm sea surface
529 temperature and reduced sea ice on the extreme circulation over the extratropical

North Pacific and North America during the 2013–2014 boreal winter. Geophysical Research Letters 42(5): 1612-1618.

Li C, Stevens B, Marotzke J. 2015. Eurasian winter cooling in the warming hiatus of 1998–2012. Geophysical Research Letters 42(19): 8131-8139.

Liu J, Curry JA, Wang H, Song M, Horton RM. 2012. Impact of declining Arctic sea ice on winter snowfall. Proceedings of the National Academy of Sciences 109(11): 4074-4079.

Luo D, Xiao Y, Yao Y, Dai A, Simmonds I, Franzke CL. 2016. Impact of Ural blocking on winter warm Arctic–cold Eurasian anomalies. Part I: Blocking-induced amplification. Journal of Climate 29(11): 3925-3947.

Lupo AR, Smith PJ. 1995. Climatological features of blocking anticyclones in the Northern Hemisphere. Tellus A: Dynamic Meteorology and Oceanography 47(4): 439-456.

Mann HB. 1945. Nonparametric tests against trend. Econometrica: Journal of the Econometric Society 13: 245-259.

Masato G, Hoskins BJ, Woollings T. 2013. Winter and summer Northern Hemisphere blocking in CMIP5 models. Journal of Climate 26(18): 7044-7059.

McCusker KE, Fyfe JC, Sigmond M. 2016. Twenty-five winters of unexpected Eurasian cooling unlikely due to Arctic sea-ice loss. Nature Geoscience 9(11): 838-842.

Mori M, Watanabe M, Shiogama H, Inoue J, Kimoto M. 2014. Robust Arctic sea-ice influence on the frequent Eurasian cold winters in past decades. Nature Geoscience 7(12): 869-873.

553 Nakamura T, Yamazaki K, Iwamoto K, Honda M, Miyoshi Y, Ogawa Y, Tomikawa Y,
554 Ukita J. 2016a. The stratospheric pathway for Arctic impacts on midlatitude
555 climate. Geophysical Research Letters 43(7): 3494-3501.
556 Nakamura T, Yamazaki K, Honda M, Ukita J, Jaiser R, Handorf D, Dethloff K. 2016b.
557 On the atmospheric response experiment to a Blue Arctic Ocean. Geophysical
558 Research Letters 43(19), doi: 10.1002/2016GL070526.
559 Outten S, Esau I. 2012. A link between Arctic sea ice and recent cooling trends over
560 Eurasia. Climatic Change 110(3-4): 1069-1075.
561 Overland J, Francis JA, Hall R, Hanna E, Kim S-J, Vihma T. 2015. The Melting Arctic
562 and Midlatitude Weather Patterns: Are They Connected? Journal of Climate
563 28(20): 7917-7932.
564 Overland J, Hanna E, Hassen-Bauer I, Kim S, Walsh J, Wang M, Bhatt U, Thoman R.
565 2016a. Surface air Temperature. In Arctic report card: update for 2016.
566 http://www.arctic.noaa.gov/Report-Card/Report-Card-
567 2016/ArtMID/5022/ArticleID/271/Surface-Air-Temperature.
568 Overland J, Dethloff K, Francis J, Hall R, Hanna E, Kim S-J, Screen J, Shepherd TG,
569 Vihma T. 2016b. Nonlinear response of mid-latitude weather to the changing
570 Arctic. Nature Climate Change 6: 992-999.
571 Overland JE, Adams JM, Bond NA. 1999. Decadal variability of the Aleutian Low and
572 its relation to high-latitude circulation. Journal of Climate 12(5): 1542-1548.
573 Overland JE, Wood KR, Wang M. 2011. Warm Arctic-cold continents: climate impacts
574 of the newly open Arctic Sea. Polar Research 30(1), doi:
575 10.3402/polar.v30i0.15787.

576 Pedersen RA, Cvijanovic I, Langen PL, Vinther BM. 2016. The Impact of Regional
577 Arctic Sea Ice Loss on Atmospheric Circulation and the NAO. Journal of Climate
578 29(2): 889-902, doi: 10.1175/jcli-d-15-0315.1.
579 Peings Y, Magnusdottir G. 2014. Forcing of the wintertime atmospheric circulation by
580 the multidecadal fluctuations of the North Atlantic ocean. Environmental Research
581 Letters 9(3): 034018.
582 Petoukhov V, Semenov VA. 2010. A link between reduced Barents□Kara sea ice and
583 cold winter extremes over northern continents. Journal of Geophysical Research:
584 Atmospheres 115(D21).
585 Poli P, Hersbach H, Dee DP, Berrisford P, Simmons AJ, Vitart F, Laloyaux P, Tan DG,
586 Peubey C, Thépaut J-N. 2016. ERA-20C: An Atmospheric Reanalysis of the
587 Twentieth Century. Journal of Climate 29(11): 4083-4097.
588 Rimbu N, Lohmann G. 2011. Winter and summer blocking variability in the North
589 Atlantic region–evidence from long-term observational and proxy data from
590 southwestern Greenland. Climate of the Past 7(2): 543-555.
591 Rimbu N, Lohmann G, Ionita M. 2014. Interannual to multidecadal Euro□Atlantic
592 blocking variability during winter and its relationship with extreme low
593 temperatures in Europe. Journal of Geophysical Research: Atmospheres 119(24):
594 13621–13636, doi: 10.1002/2014JD021983.
595 Scherrer SC, Croci-Maspoli M, Schwierz C, Appenzeller C. 2006. Two-dimensional
596 indices of atmospheric blocking and their statistical relationship with winter climate
597 patterns in the Euro-Atlantic region. International journal of climatology 26(2):
598 233-250.

599 Screen JA, Simmonds I. 2010. The central role of diminishing sea ice in recent Arctic
600 temperature amplification. Nature 464(7293): 1334.
601 Semenov VA, Bengtsson L. 2003. Modes of the wintertime Arctic temperature
602 variability. Geophysical Research Letters 30(15).
603 Semenov VA, Latif M. 2015. Nonlinear winter atmospheric circulation response to
604 Arctic sea ice concentration anomalies for different periods during 1966–2012.
605 Environmental Research Letters 10(5): 054020.
606 Semenov VA. 2016. Link between anomalously cold winters in Russia and sea-ice
607 decline in the Barents Sea. Izvestiya, Atmospheric and Oceanic Physics 52(3): 225-
608 233.
609 Serreze M, Barrett A, Stroeve J, Kindig D, Holland M. 2009. The emergence of surface-
610 based Arctic amplification. The Cryosphere 3(1): 11-19.
611 Shepherd TG. 2016. Effects of a warming Arctic. Science 353(6303): 989-990.
612 Sun L, Perlwitz J, Hoerling M. 2016. What caused the recent "Warm Arctic, Cold
613 Continents" trend pattern in winter temperatures? Geophysical Research Letters
614 43(10): 5345-5352.
615 Tang Q, Zhang X, Yang X, Francis JA. 2013. Cold winter extremes in northern
616 continents linked to Arctic sea ice loss. Environmental Research Letters 8(1):
617 014036, doi: 10.1088/1748-9326/8/1/014036.
618 Thompson DM, Cole JE, Shen GT, Tudhope AW, Meehl GA. 2015. Early twentieth-
619 century warming linked to tropical Pacific wind strength. Nature Geoscience 8(2):
620 117-121.
621 Tibaldi S, Molteni F. 1990. On the operational predictability of blocking. Tellus A:
622 Dynamic Meteorology and Oceanography 42(3): 343-365.

623 Tokinaga H, Xie S-P, Mukougawa H. 2017. Early 20th-century Arctic warming
624 intensified by Pacific and Atlantic multidecadal variability. Proceedings of the
625 National Academy of Sciences 114(24): 6227–6232, doi:
626 10.1073/pnas.1615880114.
627 Van Oldenborgh GJ, Haarsma R, De Vries H, Allen MR. 2015. Cold extremes in North
628 America vs. mild weather in Europe: The winter of 2013–14 in the context of a
629 warming world. Bulletin of the American Meteorological Society 96(5): 707-714.
630 Vavrus SJ, Wang F, Martin JE, Francis JA, Peings Y, Cattiaux J. 2017. Changes in
631 North American Atmospheric Circulation and Extreme Weather: Influence of
632 Arctic Amplification and Northern Hemisphere Snow Cover. Journal of Climate
633 30(11): 4317-4333, doi: 10.1175/jcli-d-16-0762.1.
634 Wallace JM, Held IM, Thompson DW, Trenberth KE, Walsh JE. 2014. Global warming
635 and winter weather. Science 343: 729-730.
636 Walsh JE. 2014. Intensified warming of the Arctic: Causes and impacts on middle
637 latitudes. Global and Planetary Change 117: 52-63.
638 Wiedenmann JM, Lupo AR, Mokhov II, Tikhonova EA. 2002. The climatology of
639 blocking anticyclones for the Northern and Southern Hemispheres: Block intensity
640 as a diagnostic. Journal of Climate 15(23): 3459-3473.
641 Wood KR, Overland JE. 2010. Early 20th century Arctic warming in retrospect.
642 International Journal of Climatology 30(9): 1269-1279.
643 Woollings T, Harvey B, Masato G. 2014. Arctic warming, atmospheric blocking and
644 cold European winters in CMIP5 models. Environmental Research Letters 9(1):
645 014002.

646 Wu Y, Smith KL. 2016. Response of Northern Hemisphere midlatitude circulation to
647 Arctic amplification in a simple atmospheric general circulation model. Journal of
648 Climate 29(6): 2041-2058.
649 Xie Z, Bueh C. 2017. Cold vortex events over Northeast China associated with the
650 Yakutsk□Okhotsk blocking. International Journal of Climatology 37(1): 381-398.
651 Yamanouchi T. 2011. Early 20th century warming in the Arctic: A review. Polar
652 science 5(1): 53-71.
653 Yao Y, Luo D, Dai A, Simmonds I. 2017. Increased Quasi Stationarity and Persistence
654 of Winter Ural Blocking and Eurasian Extreme Cold Events in Response to Arctic
655 Warming. Part I: Insights from Observational Analyses. Journal of Climate 30(10):
656 3549-3568, doi: 10.1175/jcli-d-16-0261.1.
657 Yue S, Pilon P, Phinney B, Cavadias G. 2002. The influence of autocorrelation on the
658 ability to detect trend in hydrological series. Hydrological processes 16(9): 1807-
659 1829.
660 Yue S, Wang C. 2004. The Mann-Kendall test modified by effective sample size to
661 detect trend in serially correlated hydrological series. Water resources management
662 18(3): 201-218.
663 Zappa G, Masato G, Shaffrey L, Woollings T, Hodges K. 2014. Linking Northern
664 Hemisphere blocking and storm track biases in the CMIP5 climate models.
665 Geophysical Research Letters 41(1): 135-139.
666 Zhang J, Tian W, Chipperfield MP, Xie F, Huang J. 2016. Persistent shift of the Arctic
667 polar vortex towards the Eurasian continent in recent decades. Nature Climate
668 Change **6**(12): 1094-1099.

669

Figure Captions

Figure 1. Trends in DJF 2-m temperature over the AA1 (a) and AA2 (b) periods from ERA20C, with only trends above the 95% confidence level plotted. Units: °C per decade. The two black circles denote the 30°N and 60°N latitudes.

Figure 2. Trends in DJF latitudinal 1000-500 hPa thickness gradient over the AA1 (a) and AA2 (b) periods, with only trends above the 95% confidence level plotted. Units: m/lat per decade. The two black circles denote the 30°N and 60°N latitudes.

Figure 3. ERA20C latitude-height cross-section of trends in DJF zonal-mean zonal winds over the AA1 (a) and AA2 (b) periods (top); trends in DJF zonal wind component at 500hPa over the AA1 (c) and AA2 (d) periods (bottom). Units: m/s per decade, with only trends above the 95% confidence level plotted. The two black circles denote the 30°N and 60°N latitudes in (c) and (d).

Figure 4. Trends in DJF |MCI| over the AA1 (a) and AA2 (b) periods, with only trends above the 95% confidence level plotted. Units: |MCI| value per decade. The two black circles denote the 30°N and 60°N latitudes.

Figure 5. Trends in DJF BF (top) and BI (bottom) over the AA1 (a, c) and AA2 (b, d) periods. Units: percentage of blocked days with respect to total days per decade and BI value per decade. Black dots indicate the area where trends are above the 95% confidence level. The two black circles denote the 30°N and 60°N latitudes. In all panels, only values where BF climatology exceeds 1% are plotted.

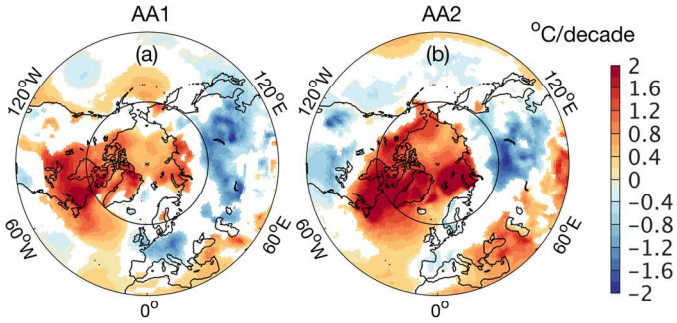

Figure 1. Trends in DJF 2-m temperature over the AA1 (a) and AA2 (b) periods from ERA20C, with only trends above the 95% confidence level plotted. Units: °C per decade. The two black circles denote the 30°N and 60°N latitudes.

148x111mm (300 x 300 DPI)

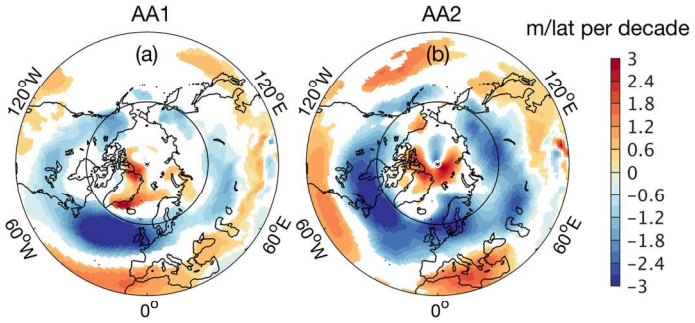

Figure 2. Trends in DJF latitudinal 1000-500 hPa thickness gradient over the AA1 (a) and AA2 (b) periods, with only trends above the 95% confidence level plotted. Units: m/lat per decade. The two black circles denote the 30°N and 60°N latitudes.

148x111mm (300 x 300 DPI)

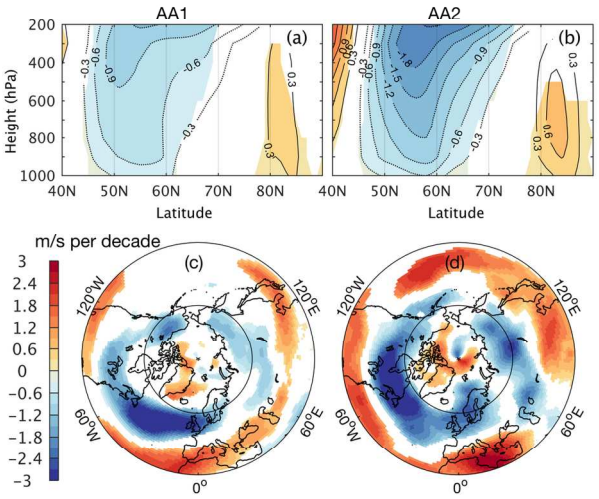

Figure 3. ERA20C latitude-height cross-section of trends in DJF zonal-mean zonal winds over the AA1 (a) and AA2 (b) periods (top); trends in DJF zonal wind component at 500hPa over the AA1 (c) and AA2 (d) periods (bottom). Units: m/s per decade, with only trends above the 95% confidence level plotted. The two black circles denote the 30°N and 60°N latitudes in (c) and (d).

148x111mm (300 x 300 DPI)

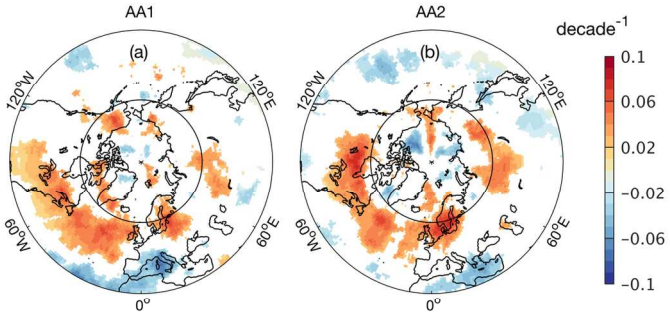

Figure 4. Trends in DJF |MCI| over the AA1 (a) and AA2 (b) periods, with only trends above the 95% confidence level plotted. Units: |MCI| value per decade. The two black circles denote the 30°N and 60°N latitudes.

148x111mm (300 x 300 DPI)

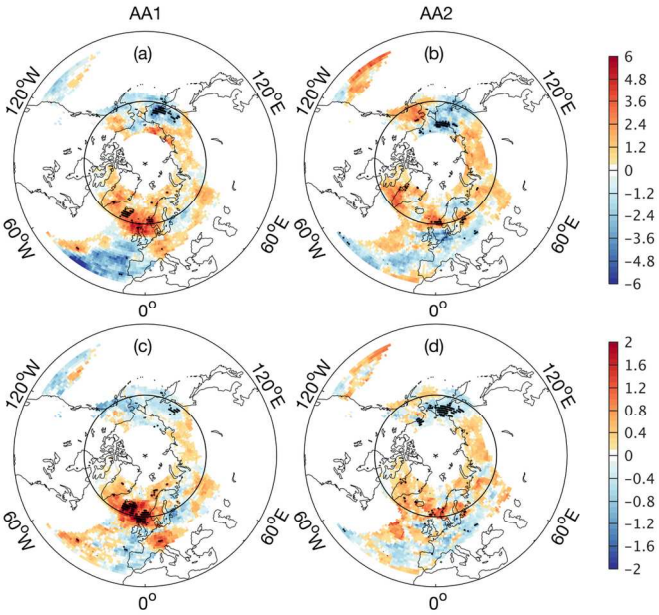

Figure 5. Trends in DJF BF (top) and BI (bottom) over the AA1 (a, c) and AA2 (b, d) periods. Units: percentage of blocked days with respect to total days per decade and BI value per decade. Black dots indicate the area where trends are above the 95% confidence level. The two black circles denote the 30°N and 60°N latitudes. In all panels, only values where BF climatology exceeds 1% are plotted.

148x111mm (300 x 300 DPI)

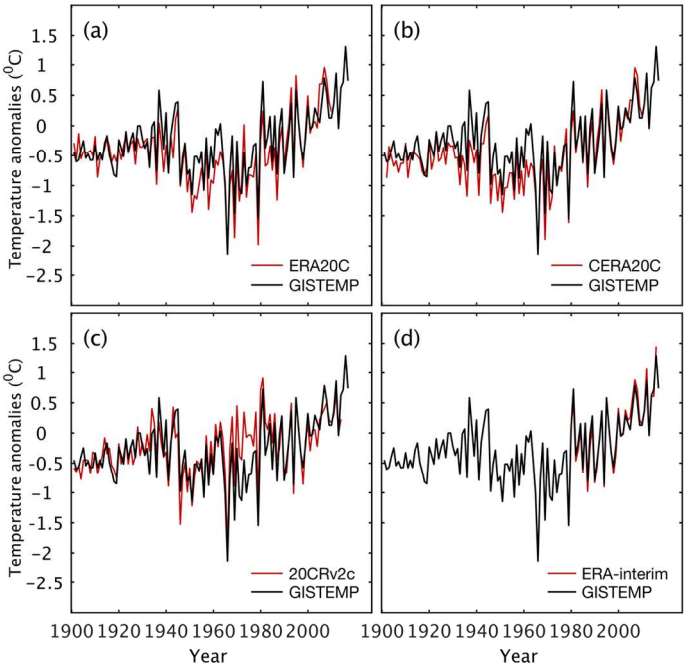

Figure S1. The area-weighted mean of 2-m air temperature anomalies in the area of 0°-360°E, 60°-90°N relative to the mean over the period of 1981-2010. This is shown as a comparison between GISTEMP (black line) and reanalysis products (red line) from (a) ERA20C, (b) CERA20C, (c) 20CRv2c and (d) ERA-interim.

148x111mm (300 x 300 DPI)

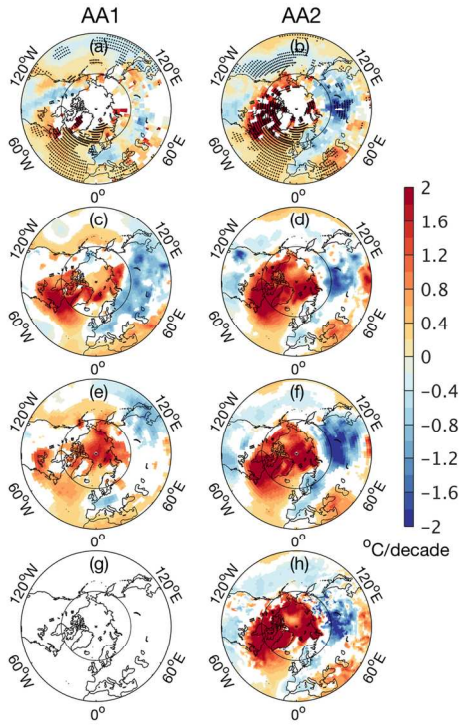

Figure S2. Trends in DJF temperature over the AA1 (left column) and AA2 (right column) periods from (a, b) GISTEMP, (c, d) CERA20C, (e, f) 20CRv2c and (g, h) ERA-interim. Units: °C per decade. The two black circles denote the 30°N and 60°N latitudes. Only trends above the 95% confidence level are plotted in (c), (d), (e), (f), (h). In (a) and (b), black dots indicate the area where trends are above the 95% confidence level, and blank areas denote missing value.

148x111mm (300 x 300 DPI)

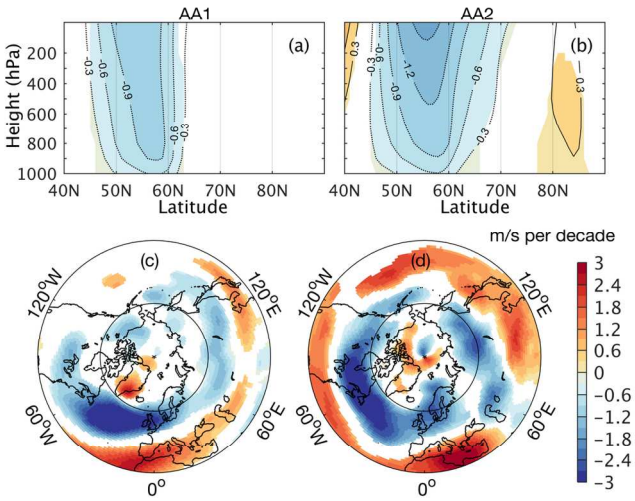

Figure S3. Same as Figure 3, but for CERA20C.

148x111mm (300 x 300 DPI)

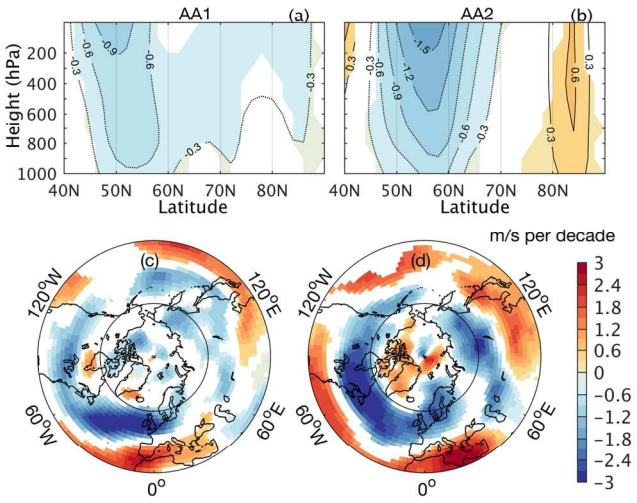

Figure S4. Same as Figure 3, but for 20CRv2c.

148x111mm (300 x 300 DPI)

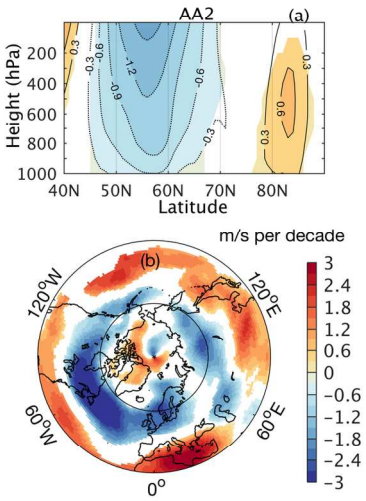

Figure S5. Same as Figure 3, but for ERA-interim during the AA2 period.

148x111mm (300 x 300 DPI)

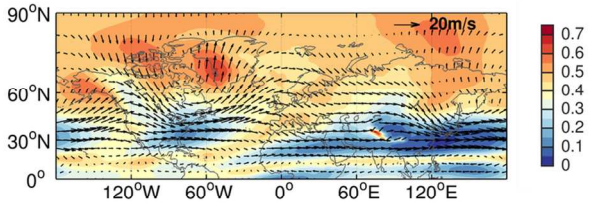

Figure S6. NH DJF climatological mean of |MCI| and 500hPa wind fields during 1901-2010.

111x83mm (300 x 300 DPI)

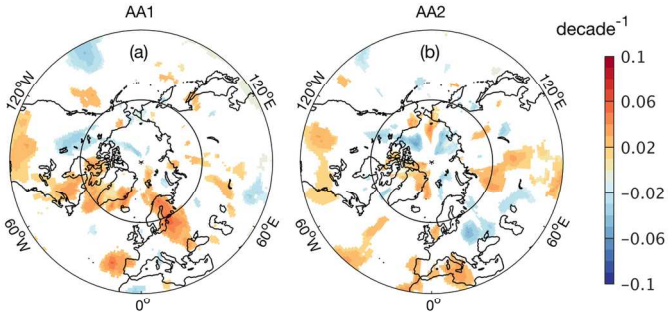

Figure S7. Trends in DJF |MCI*| (u held constant) over the AA1 (a) and AA2 (b) periods, with only trends above the 95% confidence level plotted. Units: |MCI*|value per decade. The two black circles denote the 30°N and 60°N latitudes.

148x111mm (300 x 300 DPI)

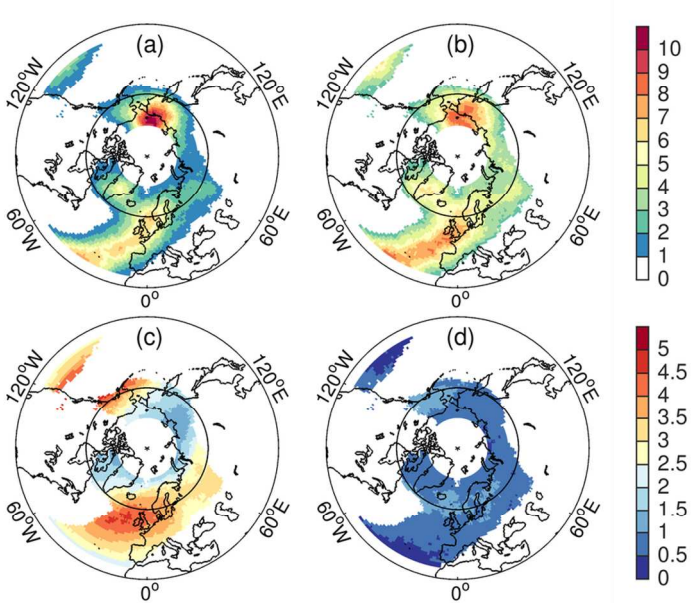

Figure S8. DJF BF (a) and BI (c) climatology for the period of 1901-2010. Units are percentage of blocked days in the total number of days per season and BI value per season, respectively. (b) and (d) are the standard deviation of BF and BI. Note that 1% BF corresponds to about one blocked day per season. Only values where BF exceeds 1% are plotted. The two black circles denote the 30°N and 60°N latitudes.

111x83mm (300 x 300 DPI)

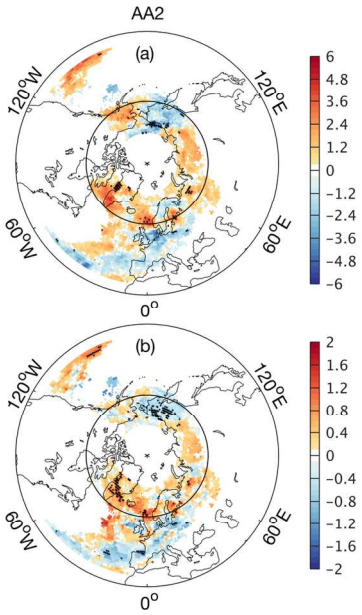

Figure S9. Same as Figure 5, but for ERA-interim during the AA2 period.

148x111mm (300 x 300 DPI)

Title: The 'Warm-Arctic/Cold-Continents' pattern during 1901-2010

Linling CHEN*, Jennifer FRANCIS, Edward HANNA

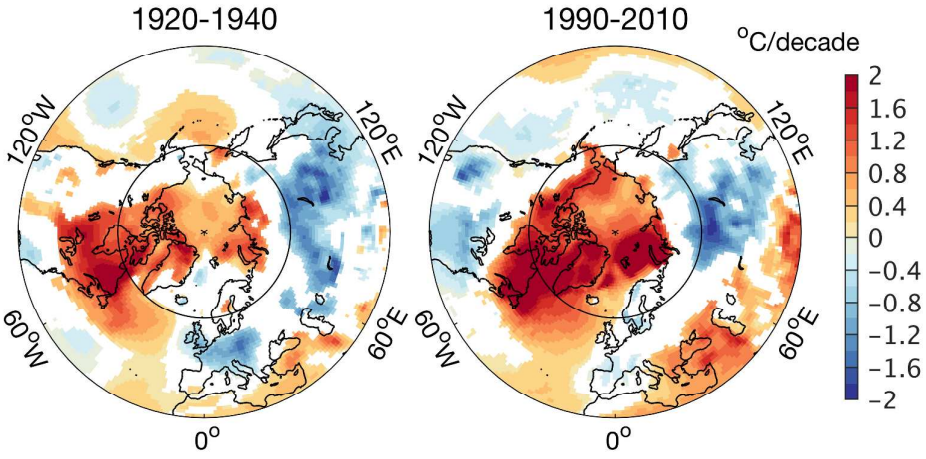

- 'Warm-Arctic/Cold-Continents' (WACC) winter weather pattern is clearly shown in both 1920-1940 and 1990-2010 periods.
- Significant weakening in mid-latitude poleward temperature gradient and zonal wind, wavier upper level flow character, and strong regional blocking frequency/intensity changes are detected during both periods.
- Noticeable regional differences of trends in these dynamical features between AA1 and AA2 period suggest the need for a more in-depth dynamical meteorological investigation of regional mechanisms of AA and mid-latitude weather linkages.